Neutron diffraction and ^{119}Sn Mössbauer spectroscopy study of Mn_3Sn_2

T. Mazet,* Q. Recour, and B. Malaman
Institut Jean Lamour, Département P2M, CNRS (UMR 7198), Nancy Université, BP 70239, 54506 Vandoeuvre-lès-Nancy Cedex, France
(Received 2 April 2010; revised manuscript received 4 May 2010; published 26 May 2010)

The temperature dependence of the magnetic structure of Mn_3Sn_2 has been determined down to 2 K from powder neutron diffraction and ^{119}Sn Mössbauer spectroscopy experiments. The Mn_3Sn_2 compound crystallizes with the Ni_3Sn_2 type of structure (*Pnma*) which comprises two crystallographic inequivalent positions for both the Mn atoms (4*c* and 8*d*) and the Sn atoms (Sn1 and Sn2 in 4*c* positions). Below $T_{C1} \sim 262$ K, the Mn 4*c* sublattice orders ferromagnetically with magnetic moments along the *b* axis and polarizes the Mn 8*d* atoms. The Mn 8*d* sublattice cooperatively orders at $T_{C2} \sim 227$ K in a canted ferromagnetic arrangement, with the ferromagnetic component along the *b* axis and the antiferromagnetic one along the *a* axis, while the ferromagnetic order of the Mn 4*c* magnetic moments along the *b* axis is preserved. The ferromagnetic component of both Mn 4*c* and Mn 8*d* reorients toward the *c* axis below $T_t \sim 197$ K. The results are discussed in connection with previous magnetic, magnetocaloric, and specific-heat measurements. Group theory arguments indicate that the magnetic state realized below T_t should be described by a spin Hamiltonian incorporating fourth or higher-order terms in the spins or that a very small (undetected) monoclinic distortion takes place. The spin reorientation at T_t yields strong variation in the apparent quadrupolar splittings (2ε) of the two ^{119}Sn Mössbauer subspectra and allows observing anisotropic contributions to the hyperfine field. The V_{ZZ} components of the electric field gradient tensor at the Sn1 and Sn2 nuclei are found to lie in the *ac* plane and to be of opposite sign. The 5*p* charge and spin densities are both deduced to be more anisotropic on Sn2 atoms than on Sn1 atoms.

DOI: 10.1103/PhysRevB.81.174427 PACS number(s): 75.25.−j, 75.50.Cc, 76.80.+y

I. INTRODUCTION

The orthorhombic Mn_3Sn_2 compound (*Pnma*, Ni_3Sn_2 type of structure) has been shown to present promising magnetocaloric properties for potential cooling applications.[1,2] The magnetic refrigeration is expected to become an alternative to traditional gas compression technology because of its higher efficiency and the lack of ozone depleting or greenhouse effect gas.[3–5] It relies on the magnetocaloric effect (MCE), which is the magnetic entropy change (ΔS_M) or adiabatic temperature change (ΔT_{ad}) of a magnetic solid in a varying magnetic field.[3–5] There is currently an intense research activity for identifying materials having interesting magnetocaloric properties for applications.[3–5] Mn_3Sn_2 undergoes two successive ferromagneticlike transitions at $T_{C1} \sim 262$ K and $T_{C2} \sim 227$ K which yield a two-peak magnetocaloric response covering a broad temperature interval ($\sim$200–300 K).[1,2] This large extend of the MCE together with the abundance of the raw elements make Mn_3Sn_2 an interesting candidate for potential applications, despite the moderate magnitude of its MCE maxima (about one-third that of Gd).

The Mn_3Sn_2 compound was for a long time somewhat disregarded. Its magnetic properties have been precisely determined only recently, concomitantly to part of its magnetocaloric properties.[1] Mn_3Sn_2 has also been investigated by specific-heat measurements,[2] another macroscopic technique, but microscopic information about its spin structures are still missing. This relative ignorance of the magnetic properties of such a simple binary phase likely originates from an improper knowledge of the Mn-Sn phase diagram near 60% atomic Mn composition, which has often led to erroneous assignation of the sample composition and/or crystal structure even in recent publications (see, e.g., Ref. 6). In this region of the Mn-Sn phase diagram, a single "Mn_2Sn" phase, stable from low-temperature up to its peritectoidal decomposition, was reported (see, e.g., Ref. 7). The study of Stange *et al.*[8] has clearly shown that there are in fact two different phases with slightly different Mn contents: the high-temperature (480 °C$<T<$880 °C) nonstoichiometric $Mn_{2-x}Sn$ alloy ($0.18 \leq x \leq 0.34$) and the low-temperature ($T<540$ °C) Mn_3Sn_2 line compound. The $Mn_{2-x}Sn$ phase, whose homogeneity range evolves with temperature, crystallizes in a hexagonal structure ($P6_3/mmc$) intermediate between the hexagonal NiAs and Ni_2In types of structure (Fig. 1) by partial filling of the Sn trigonal bipyramids. The Mn_3Sn_2 compound is isotypic with Ni_3Sn_2 (*Pnma*). Its crystal structure (Fig. 1), which comprises two Mn and two Sn crystallographic positions, can be described as an orthorhombically deformed partially filled NiAs structure. In the *Pnma* setting, the orthorhombic cell parameters are related to the hexagonal ones as follows: $a \sim \sqrt{3}a_h$, $b \sim c_h$, and $c \sim 2a_h$, i.e., the *ac* plane of the orthorhombic cell corresponds to the basal *ab* plane of the hexagonal cell. The claims of Stange *et al.*[8] are corroborated by the crystallographic study of Elding-

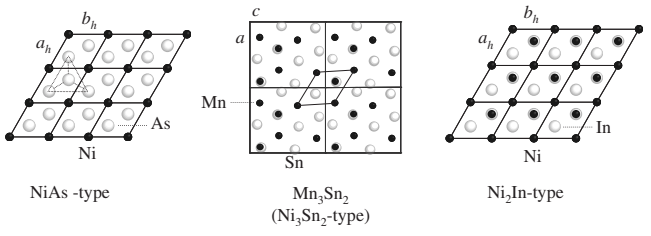

FIG. 1. Projection of the of the crystal structures of NiAs, Mn_3Sn_2 (Ni_3Sn_2-type) and Ni_2In.

Pontén *et al.*[9] and by our own experience on these systems.

In the present work, we use powder neutron diffraction and ^{119}Sn Mössbauer spectroscopy experiments to determine the magnetic structures of Mn_3Sn_2 and to shed light on the nature of the three magnetic transitions that it undergoes. The transition at $T_{C1} \sim 262$ K is unambiguously a typical paramagnetic to ferromagnetic second-order transition,[1] as attests for instance the field dependence of the corresponding lambda-type anomaly in the specific-heat curves.[2] The transition at $T_{C2} \sim 227$ K is also ferromagneticlike. The lack of thermal and field hysteresis in the magnetization data,[1] as well as the broad but somewhat unusual peak in the specific-heat data,[2] suggests classifying it as a second-order transition. This is not very common for what might *a priori* be an order-order transformation. Besides these two ferromagneticlike transitions, there is a third transition at $T_t \sim 197$ K that has been tentatively ascribed to the appearance of a weak antiferromagnetic interaction.[1] It corresponds to a maximum in the low-field magnetization data[1] and yields a little anomaly in the zero-field specific-heat data.[2] In the whole ordered temperature range, the isothermal magnetization curves look like that of a simple ferromagnet.[1] The maximal magnetization at 2 K points to an average atomic Mn magnetic moment of $\sim 1.8 \mu_B$.[1]

II. EXPERIMENTAL DETAILS

The powder sample (~ 4 g) was prepared as described in Ref. 1. Sample composition and purity were checked by microprobe analysis (Cameca SX 100) and x-ray powder diffraction experiments (Philips X'Pert Pro Diffractometer, $\lambda_1 = 1.540\,56$ Å and $\lambda_2 = 1.544\,39$ Å). Besides the main Mn_3Sn_2 phase, the sample also contains small amounts (~ 5 wt. %) of the antiferromagnetic MnO ($T_N \sim 120$ K) (Ref. 10) and $MnSn_2$ ($T_N \sim 330$ K) (Ref. 11) impurities. Neutron diffraction experiments were performed at the Institut Laue Langevin (Grenoble France) using the D1B two-axis diffractometer ($\lambda = 2.52$ Å). This diffractometer spans an angular range of 80° (2θ from 16° to 96° in the present experiments) and has a position sensitive detector of 400 channels. Diffraction patterns were collected every 2 K from 2 to 300 K thanks to a standard helium cryostat. Longer exposure time measurements were performed at several selected temperatures. A few patterns were also recorded under magnetic field ($\mu_0 H \leq 1.5$ T) thanks to an electromagnet. The neutron patterns were analyzed by Rietveld profile refinements using the program Fullprof.[12] The shape of the diffraction peaks was fitted using a pseudo-Voigt function. Besides the peak profile parameters, the fits comprised scale factor, zero shift, cell parameters, crystallographic position parameters, and magnetic parameters (see below for details). The R_n and R_m are the Bragg agreement factors calculate for, respectively, the nuclear and magnetic contribution to the diffraction pattern while R_{wp} is the Rietveld agreement factor corresponding to the weight profile factor as defined in Ref. 13.

The ^{119}Sn Mössbauer measurements were carried out using a constant-acceleration spectrometer in standard transmission geometry. Several spectra were recorded between 300 and 5 K in a liquid helium cryostat. The velocity scale was calibrated with a ^{57}CoRh source (25 mCi) and a metallic iron foil at room temperature. We used a Ba $^{119\,m}SnO_3$ source (10 mCi) kept at room temperature which also served as the reference for the isomer shifts. A polycrystalline absorber with natural abundance of ^{119}Sn isotope and thickness of ~ 15 mg cm^{-2} was used. A palladium foil of 0.5 mm thickness was used as a critical absorber for tin x rays. The Mössbauer spectra were fitted with a least-squares method program assuming Lorentzian peaks.[14]

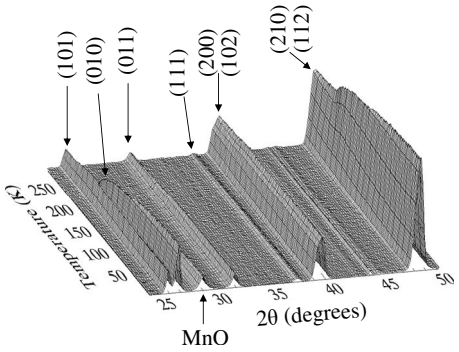

FIG. 2. Selected angular region ($25° \leq 2\theta \leq 50°$) of the neutron thermodiffractogram of Mn_3Sn_2.

III. EXPERIMENTAL RESULTS AND INTERPRETATION

A. Neutron diffraction

A representative part ($25° \leq 2\theta \leq 50°$) of the neutron thermodiffractogram of Mn_3Sn_2 recorded in the 2–300 K temperature range is shown in Fig. 2. During the experiments, it has been checked that no magnetic peak appears in the low-angles region.

The refinements of the nuclear structure, which has led to low R nuclear (R_n) factor (2–4 %), indicate that the Ni_3Sn_2 type of structure (*Pnma*) is kept down to 2 K. In addition, within the accuracy of the measurements, the thermal variation in the refined cell parameters (not shown) does not reveal anomaly at the magnetic transitions. The crystal parameters derived from the room-temperature data (top panel of Fig. 3) are given in Table I. They are in good agreement with those given in Ref. 8.

From room temperature down to $T_{C2} \sim 227$ K, only reflections corresponding to the *Pnma* space group are observed (Figs. 2 and 3). Below $T_{C2} \sim 227$ K the anti-n (010) diffraction peak appears (Figs. 2 and 3). The peak which growths below $T \sim 120$ K at $2\theta = 28.7°$ is due to the antiferromagnetic ordering of the MnO impurity (Figs. 2 and 3). Hence, in the whole magnetically ordered temperature range the magnetic structure of Mn_3Sn_2 is commensurate associated with the propagation vector $\mathbf{k} = (0\ 0\ 0)$.

To help solving the magnetic structure of Mn_3Sn_2 we use group theory analysis.[15,16] Since Mn_3Sn_2 presents a spontaneous magnetization in its whole magnetically ordered state, the relevant magnetic space groups (i.e., irreducible representations Γ_i) are those containing a ferromagnetic mode. The magnetic modes of the two inequivalent Mn positions

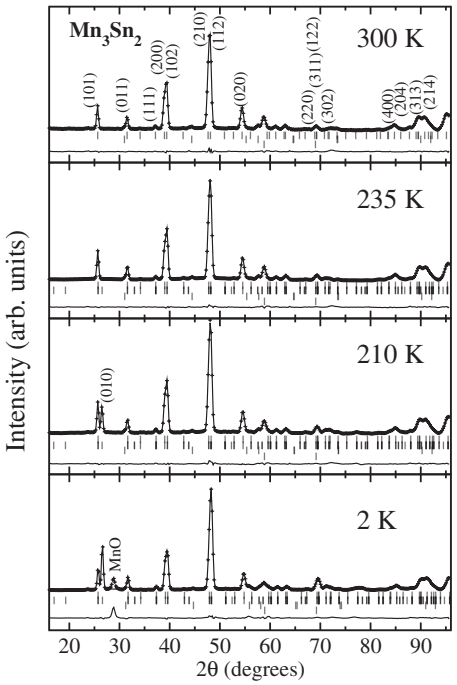

FIG. 3. Observed and calculated neutron-diffraction patterns of Mn_3Sn_2 at 300, 235, 210, and 2 K. The vertical lines indicate the angular positions of the nuclear and magnetic reflections (top) as well as those due to the nuclear contribution from the MnO and $MnSn_2$ impurities (bottom).

(8*d* and 4*c*) of the three possible magnetic space groups of *Pnma* associated with the wave vector $\mathbf{k}=(0\ 0\ 0)$ and having a ferromagnetic mode are given in Table II. We use the numbering of atoms and the notation given in Ref. 17.

Upon cooling below $T_{C1}\sim 262$ K, the diffracted intensity of a few peaks—namely, (101), (011), (210)+(112)—is slightly modified (Figs. 3 and 4). At $T=235$ K (Fig. 3), the best refinements indicate that the Mn 4*c* and Mn 8*d* magnetic moments are in F_y and F_{By} configuration, respectively (Table III), without component along the *x* or *z* direction. Hence, for $T_{C1}\geq T\geq T_{C2}$, Mn_3Sn_2 is a simple collinear ferromagnet described in the magnetic space group *Pn′ma′* with the Mn moments of both the 4*c* and 8*d* positions pointing along the *b* axis (Fig. 5). The refined parameters at 235 K are given in Table III. We note that the refined Mn moment at the 4*c* position $[m_{\mathrm{Mn}\,4c}=1.53(7)\mu_B]$ is significantly larger than that of Mn 8*d* $[m_{\mathrm{Mn}\,8d}=0.83(4)\mu_B]$.

TABLE I. Atomic positions and cell parameters of Mn_3Sn_2 (*Pnma*) from room-temperature neutron data.

Atom	Position	*x*	*y*	*z*
Mn1	8*d*	0.2245(11)	0.0036(16)	0.1229(22)
Mn2	4*c*	0.9079(14)	1/4	0.1299(16)
Sn1	4*c*	0.5969(9)	1/4	0.6426(14)
Sn2	4*c*	0.5610(9)	1/4	0.0932(10)
$a=7.5646(10)$ Å; $b=5.5099(6)$ Å; $c=8.5975(12)$ Å				
$B_{iso}=1.15(8)$ Å^2; $R_n=2.8\%$; $R_{wp}=5.7\%$				

Below $T_{C2}\sim 227$ K, the anti-*n* (010) reflection starts to growth and the intensity of the (210)+(112) peaks strongly increases (Figs. 2 and 4). The occurrence of the (010) reflection indicates that the magnetic space group contains the *n′* antielement, which limits the choice to *Pn′m′a* and *Pn′ma′*, and that the Mn moments are no longer all strictly collinear to the *b* axis. The purely magnetic (010) reflection is due to the antiferromagnetic A_{Bx} mode of 8*d* atoms and there is no component along the *c* axis. The magnetic structure for $T_{C2}\geq T\geq T_t$ has been determined to be a canted arrangement still described in the magnetic space group *Pn′ma′* with F_y and $A_{Bx}F_{By}$ magnetic modes for the Mn 4*c* and Mn 8*d* magnetic moments, respectively (Table III). Thus, in this temperature range, the magnetic structure of Mn_3Sn_2 is built upon ferromagnetic (010) Mn planes with the Mn 4*c* moments along the *b* axis while those of Mn 8*d* deviate from the *b* axis to form a canted arrangement (Fig. 5). The refined parameters at 210 K are given in Table III. The canting angle of the Mn 8*d* moments with respect to the *b* axis is ~51° and remains almost constant down to T_t. At 210 K, the magnetic moment on Mn 8*d* atoms $[m_{\mathrm{Mn}\,8d}=1.90(4)\mu_B]$ is now a little larger than that of Mn 4*c* atoms $[m_{\mathrm{Mn}\,4c}=1.79(6)\mu_B]$.

Below $T_t\sim 197$ K the magnetic intensity of some ferromagnetic reflections evolve again while the thermal dependence of the (010) and (210)+(112) lines does not present any anomaly (Figs. 2 and 4). No further change is observed down to 2 K. The refinements carried out below T_t lead to the conclusion that the ferromagnetic component of both the Mn 4*c* and Mn 8*d* sites has reoriented along the *c* axis while the antiferromagnetic component on Mn 8*d* atoms is still along the *a* axis and described by the A_{Bx} mode. This means that different magnetic space groups (i.e., irreducible representations Γ_i) are involved: *Pn′m′a* (F_z and F_{Bz} for Mn 4*c* and Mn 8*d*, respectively) and *Pn′ma′* (A_{Bx} for Mn 8*d*). The occurrence of magnetic structures described by several irreducible representations is not the most frequent situation.[15,16] This point will be discussed in details in Sec. IV. The canted ferromagnetic structure of Mn_3Sn_2 below T_t is depicted in Fig. 5. It closely resembles that occurring between T_{C2} and T_t, except that the ferromagnetic components lie along the *c* axis at low temperature. The canting angle of the Mn 8*d* magnetic moments relative to the *c* axis is constant below T_t (~51°) and nearly identical to the canting angle with the *b* axis found above T_t. The refined Mn moment components at 2 K are given in Table III. The magnetic moment carried out by the Mn atoms in 8*d* position $[m_{\mathrm{Mn}\,8d}=2.97(4)\mu_B]$ is significantly larger than that on Mn 4*c* $[m_{\mathrm{Mn}\,4c}=2.30(6)\mu_B]$. Figure 6 shows the temperature variation in the magnetic moments. The total Mn 8*d* magnetic moment markedly increases at T_{C2}, because of the appearance of the antiferromagnetic component and a moderate enlargement of its ferromagnetic component, while the Mn 4*c* magnetic moment displays standard temperature dependence below T_{C1}. No anomaly in the magnitude of the Mn moments components is detected at T_t.

A few neutron-diffraction patterns have been recorded in applied magnetic fields up to 1.5 T. Due to the numerous diffraction peaks arising from the sample environment, it was not possible to analyze the data quantitatively. Although we cannot extract quantitative results, our experiments indi-

TABLE II. The different magnetic modes of the 4*c* and 8*d* sites for the three magnetic space group (irreducible representations Γ_i) of *Pnma* associated with the propagation vector **k**=(0 0 0) and having a ferromagnetic mode (Ref. 17).

	Pn′m′a Γ_{2g}			*Pnm′a′* Γ_{3g}			*Pn′ma′* Γ_{4g}		
Position 4*c*	C_x		F_z	F_x		C_z		F_y	
1	+		+	+		+		+	
2	+		+	+		+		+	
3	−		+	+		−		+	
4	−		+	+		−		+	
Position 8*d*	G_{Bx}	C_{By}	F_{Bz}	F_{Bx}	A_{By}	G_{Bz}	A_{Bx}	F_{By}	C_{Bz}
1	+	+	+	+	+	+	+	+	+
2	−	+	+	+	−	−	−	+	+
3	+	−	+	+	−	+	−	+	−
4	−	−	+	+	+	−	+	+	−
5	+	+	+	+	+	+	+	+	+
6	−	+	+	+	−	−	−	+	+
7	+	−	+	+	−	+	−	+	−
8	−	−	+	+	+	−	+	+	−

cate that the canted ferromagnetic arrangement is not significantly modified by an applied field whatever temperature below T_t. This is illustrated in Fig. 7 where it can be observed that the intensity of the purely antiferromagnetic (010) line is visibly insensitive to the strength of the applied magnetic field at both T=2 and 210 K.

B. ^{119}Sn Mössbauer spectroscopy

In orthorhombic Mn_3Sn_2, there are two inequivalent Sn atoms (Sn1 and Sn2) at 4*c* positions. As illustrated in Fig. 8(a), both Sn atoms are located within a distorted trigonal prism of Mn 8*d* atoms. The Mn 8*d*-Sn distances range from ~2.80 to ~2.85 Å for Sn1 and from ~2.80 to ~3.10 Å for Sn2, respectively. Sn1 is in addition coordinated by three Mn 4*c* atoms—two along the *b* axis and one in the *ac* plane—at shorter distances of ~2.75 Å, while only two Mn 4*c* atoms further coordinated Sn2 in the *ac* plane at even shorter distances of ~2.60 and ~2.70 Å.

The ^{119}Sn Mössbauer spectra of Mn_3Sn_2 recorded between 300 and 5 K are shown on Fig. 9. In the paramagnetic state ($T>262$ K), a broadened and asymmetric doublet is observed. The spectra recorded using the magic-angle method[18] are identical to that obtained in normal configuration, indicating that the asymmetry of the doublet is not related to texture effects. In the magnetic state the spectra comprise two sextets characteristic of tin nuclei experiencing large hyperfine fields. There is in addition a central component due to β-Sn, which growths upon cooling due to the strong increase in the Lamb-Mössbauer *f* factor of Sn nuclei

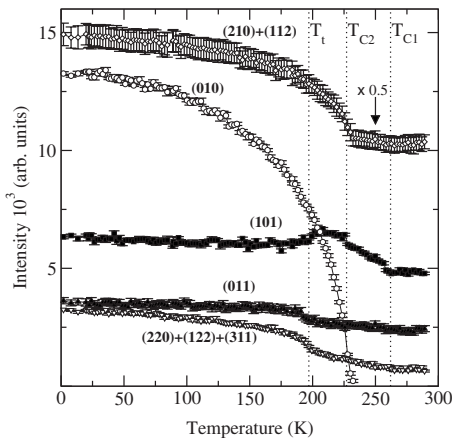

FIG. 4. Temperature dependence of the intensity of some selected peaks or groups of peaks.

TABLE III. Refined Mn 8*d* and Mn 4*c* magnetic moment components from neutron data.

		235 K	210 K	2 K
Mn 8*d*	Mode	F_{By}	$A_{Bx}F_{By}$	$A_{Bx}F_{Bz}$
	$m_x(\mu_B)$		1.49(2)	2.32(2)
	$m_y(\mu_B)$	0.83(4)	1.18(3)	
	$m_z(\mu_B)$			1.85(4)
	$m(\mu_B)$	0.83(4)	1.90(3)	2.97(3)
Mn 4*c*	Mode	F_y	F_y	F_z
	$m_x(\mu_B)$			
	$m_y(\mu_B)$	1.53(7)	1.79(6)	
	$m_z(\mu_B)$			2.30(6)
	$m(\mu_B)$	1.53(7)	1.79(6)	2.30(6)
R_{mag}, R_{wp} (%)		14.1, 6.1	8.5, 6.4	5.8, 7.7

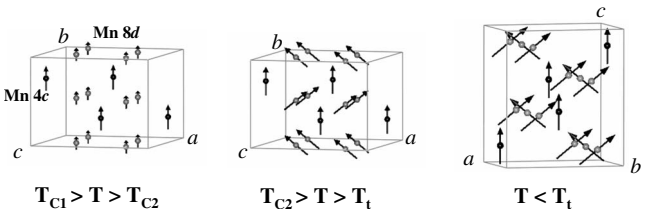

FIG. 5. Schematic representation of the magnetic structures of Mn_3Sn_2. Only the Mn atoms are drawn (Mn 8*d*: light gray; Mn 4*c*: black). For reasons of clarity the orientation of the crystal axes is changed for $T < T_t$.

in this phase.[19] A very minor part of the resonant area (~3%) is ascribed to the $MnSn_2$ impurity. The hyperfine parameters do not strictly correspond to those given in Ref. 20, but this compound is known to have a varying Sn content. Beside these impurity contributions, the spectra are satisfactorily refined by considering two subspectra of almost equal intensity, in connection with the occurrence of two inequivalent Sn sites of identical multiplicity. The line widths of the two subspectra were constrained to be the same ($\Gamma = 1.0$ to 1.2 mm s^{-1}).

Fits in the paramagnetic region yield $|\Delta p|$ values of 1.08 ± 0.04 mm s^{-1} and 1.37 ± 0.04 mm s^{-1}, where the total quadrupole splitting in the paramagnetic state Δp is given by

$$\Delta_p = \frac{eQV_{ZZ}}{2}\sqrt{\left(1+\frac{\eta^2}{3}\right)}. \quad (1)$$

A first set of fits in the magnetically ordered state was carried out in the first-order approximation. The fits allow extracting

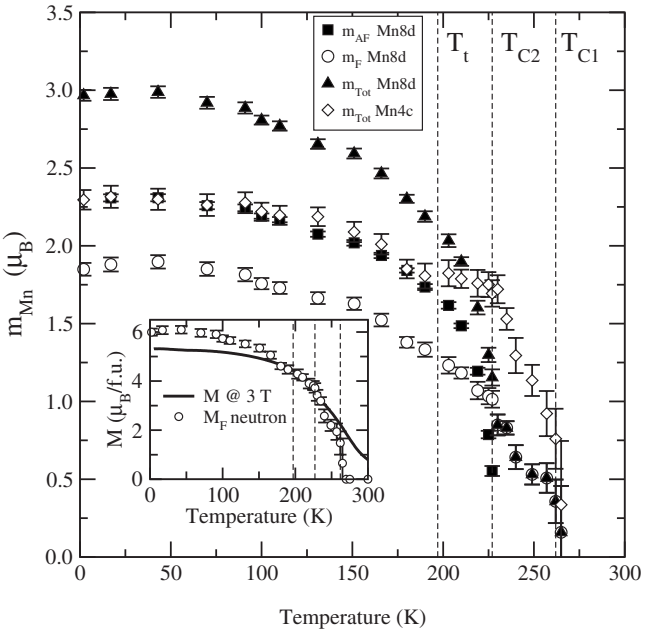

FIG. 6. Temperature dependence of the Mn magnetic moments at the 8*d* and 4*c* positions. The inset compares the temperature dependence of the zero-field magnetization from neutron data with that of the macroscopic magnetization recorded in a 3 T field (data from Ref. 1).

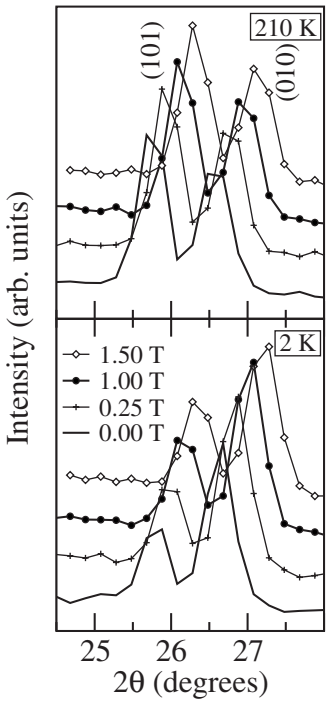

FIG. 7. Selected angular region of the observed neutron-diffraction patterns of Mn_3Sn_2 at 210 and 2 K in applied magnetic fields up to 1.5 T.

the apparent quadrupolar splitting 2ε which is related to the quadrupolar interaction $\Delta = eQV_{ZZ}/2$ by

$$2\varepsilon = \Delta\left[\frac{3\cos^2\theta - 1 + \eta\sin^2\theta\cos 2\varphi}{2}\right]. \quad (2)$$

In this equation, θ and φ are, respectively, the polar and azimuthal angles of the hyperfine field direction with respect to the electric field gradient (EFG) frame of reference.

The fitted isomer shifts (*IS*) range between 1.95 and 2.10 mm s^{-1}, typical values for metallic compounds. The

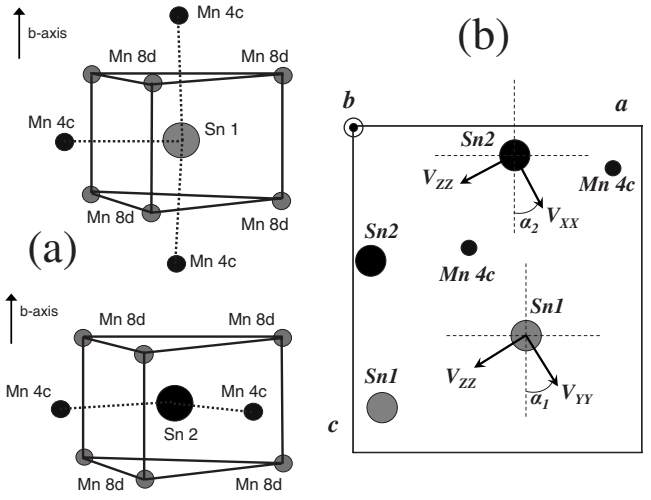

FIG. 8. (a) Atomic environment of the two Sn sites in Mn_3Sn_2. (b) Orientation of the EFG principal axes in the (x, 1/4, z) plane at the Sn1 and Sn2 sites from band structure calculations.

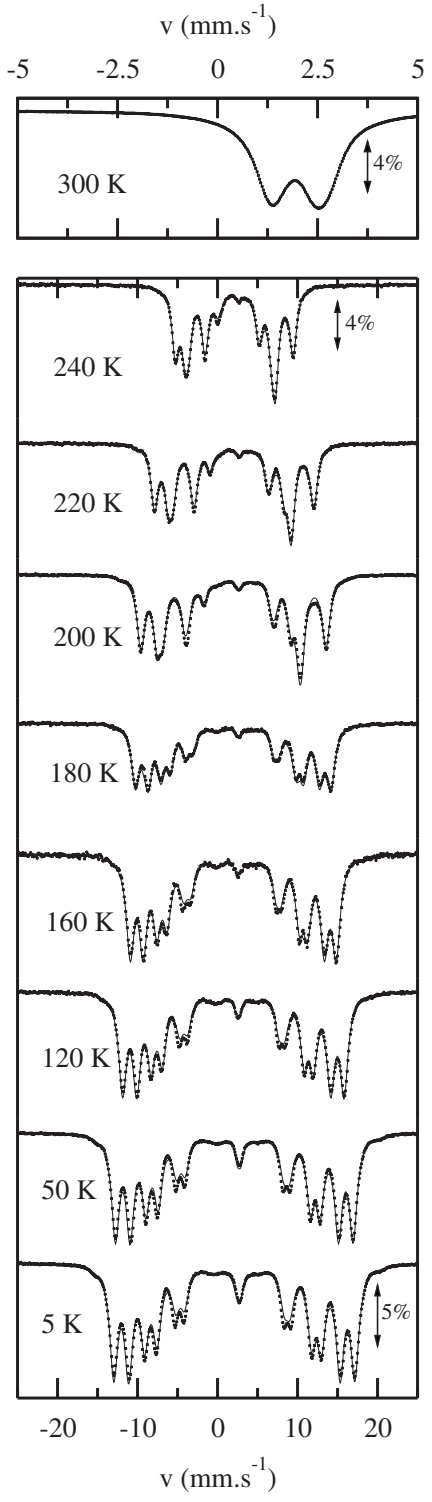

FIG. 9. Experimental ^{119}Sn Mössbauer spectra of Mn_3Sn_2 between 300 and 5 K together with their least-squares envelope (from fits carried out using the full hyperfine Hamiltonian).

temperature variation in the apparent quadrupolar splitting (2ε) and hyperfine fields (B_{hf}) of the two subspectra are shown in Fig. 10. Large B_{hf} values up to 220 kG are observed. For $T_{C1} > T > T_t$, the 2ε values, very different from each other, are found to be almost independent of temperature (approximately +0.27 and −1.06 mm s^{-1} for site 1 and

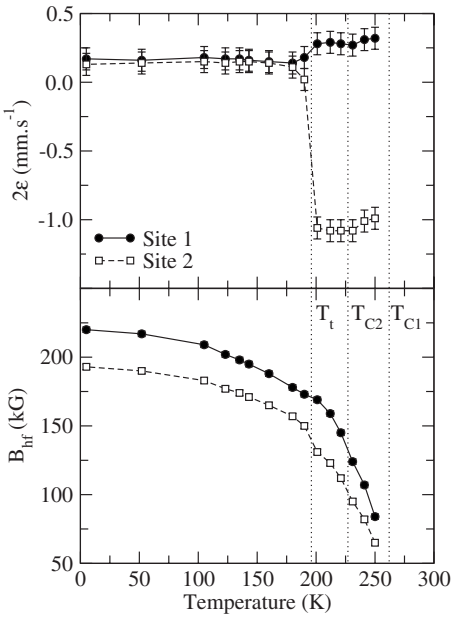

FIG. 10. Temperature dependence of the apparent quadrupolar splitting (2ε) and of the hyperfine field (B_{hf}) at the two Sn sites of Mn_3Sn_2 from fits carried out in the first-order approximation.

site 2, respectively). At T_t, the apparent quadrupolar splittings strongly change to reach almost the same value. They remain constant down to 5 K (approximately +0.17 and +0.14 mm s^{-1} for site 1 and site 2, respectively). Thus, the apparent quadrupolar splitting is unaltered at T_{C2} whereas it strongly evolves at T_t, especially for site 2. Assuming that the EFG components Δ and η do not vary significantly at the magnetic transitions, as is generally observed, the lack of change in the 2ε values at T_{C2} implies constant θ and φ values [Eq. (2)], which is consistent with the neutron study. On the contrary, the strong variation in 2ε at T_t indicates that a reorientation of the hyperfine field direction takes place at this temperature, in concordance with the Mn spins reorientation observed by neutron diffraction.

In Sn-based magnetic compounds, the hyperfine field at the nucleus of nominally diamagnetic tin atoms comes from the hybridization of the Sn valence states with the polarized states of the magnetic atoms (here Mn). This spin-dependent hybridization yields weak induced Sn magnetic moments which generate the so-called transferred hyperfine fields at the Sn nuclei (see Ref. 21 and references therein). The total hyperfine field B_{hf} comprises Fermi contact, dipolar and orbital contributions (see Refs. 21 and 22). In most cases, the dominant contribution is the isotropic Fermi contact term. It is caused by the spin-up and spin-down 5*s* charge density imbalance at the nucleus. The dipolar term arises from the nonspherical 5*p* spin density at the Sn atoms. Because of spin-orbit coupling, the spin polarization of the 5*p* states induces an orbital field. The dipolar field is expected to be larger than the orbital field. These two contributions are generally one order of magnitude lower than the Fermi contact term and are anisotropic: they depend on the neighboring Mn magnetic moments orientation and thus can change if the Mn spins reorient. The dipolar term is not necessarily collinear to the other two contributions and can make deviate the Sn

TABLE IV. ^{119}Sn hyperfine interaction parameters of Mn_3Sn_2 for $T_t<T<T_{C1}$ with fixed θ and φ values (θ=90° and φ=0° for site 1; θ=90° and φ=90° for site 2, see text). P is the relative area of the corresponding subspectrum.

T (K)	Site	P ±0.03	Γ (mm s^{-1}) ±0.06	IS (mm s^{-1}) ±0.08	Δ (mm s^{-1}) ±0.08	B_{hf} (kG) ±3	η ±0.1
250	1	0.53	1.01	1.95	−1.08	83	0.4
	2	0.47	1.01	2.06	1.28	64	0.7
240	1	0.53	1.03	1.98	−1.09	106	0.3
	2	0.47	1.03	2.06	1.21	81	0.8
230	1	0.52	1.05	1.97	−1.09	122	0.3
	2	0.48	1.05	2.07	1.25	93	0.7
220	1	0.52	1.09	1.95	−1.09	145	0.4
	2	0.48	1.09	2.09	1.21	112	0.8
210	1	0.51	1.09	1.95	−1.09	158	0.4
	2	0.49	1.09	2.08	1.17	123	0.9
200	1	0.52	1.19	1.96	−1.09	168	0.4
	2	0.48	1.19	2.06	1.18	131	0.8

hyperfine field direction from that of hybridization induced Sn moment.[20,22] Since the large Sn hyperfine fields observed in Mn_3Sn_2 are undoubtedly dominated by the isotropic Fermi contact term (see Sec. IV), we assume that the B_{hf} direction is collinear to the Sn moment. The antiferromagnetically arranged m_x component of the magnetic moment of the six Mn 8d first neighbors yields zero contribution. We consequently expect the Sn hyperfine fields to be collinear (parallel or antiparallel) to the ferromagnetic component of the Mn moments, that is along the b axis above T_t and along the c axis below this temperature. We also note that the B_{hf} magnitude is not significantly altered at T_{C2} (Fig. 10), in agreement with the neutron data which points to a limited increase in the Mn 8d ferromagnetic component at T_{C2} (Fig. 6)

To specify the θ and φ values [Eq. (2)], we further needs to know the orientation of the principal axes of the EFG tensor. From the *.m.* local symmetry at the Sn sites, it can be concluded that two of the principal axes of the EFG tensor are within the ac plane while the third one lies along the b axis, although it is not possible to know *a priori* which is the principal Z axis and to specify the orientation of the two principal axes in the ac plane. A nonzero asymmetry parameter η is expected for both sites. In the past, point charge calculations, somewhat questionable for metallic compounds, were often used to get information on the EFG axes orientation. Modern band structure calculations now offer a very reliable tool for evaluating EFG properties.[24–26] Computations using either the experimental room-temperature or low-temperature crystal parameters were performed with the Wien2k code,[27] assuming a non-spin-polarized state or various collinear magnetic configurations (ferromagnetic, antiferromagnetic, or ferrimagnetic).[28] It was found that the nature of the magnetic order hardly influences the EFG tensor components (V_{ZZ} and η), reinforcing the above assumption of an unchanged EFG at the magnetic transitions. On the other hand, the magnitude of V_{ZZ} and η significantly depends on the considered crystal parameters, though η and the absolute value of V_{ZZ} are systematically calculated to be larger for Sn2. A precise quantitative evaluation would require atomic positions relaxation. The sign of V_{ZZ} and the orientation of the EFG principal axes are however less sensitive, allowing some conclusions to be reached. In all considered cases, it has been found that (i) for Sn1, V_{ZZ} is positive and lies in the ac plane while the (necessarily negative) V_{XX} and V_{YY} components are along the b axis and in the ac plane, respectively. The principal Y and Z axes are rotated from about $\alpha_1 \sim 30-35°$ relative to the crystal c and a axes, respectively [Fig. 8(b)]. (ii) For Sn2, V_{ZZ} is also in the ac plane but with a negative sign, V_{YY} being along the b axis and V_{XX} in the ac plane. The principal X and Z axes are rotated from about $\alpha_2 \sim 25-30°$ relative to the crystal frame as shown in Fig. 8(b).

Since the quadrupole moment Q of the first excited state of the ^{119}Sn nucleus is negative,[25,29] the computations forecast the quadrupole interaction $\Delta = eQV_{ZZ}/2$ to be negative for Sn1 and positive for Sn2.

For temperatures above $T_t \sim 197$ K, the hyperfine fields at the Sn sites are along the b axis. Therefore, from the orientation of the EFG axes given above: θ=90° and φ=0° for Sn1 while θ=90° and φ=90° for Sn2. Taking into account these angle values, the only solutions consistent with both the $|\Delta p|$ and 2ε values (see Ref. 30) imply to associate site 2 ($2\varepsilon \sim -1.06$ mm s^{-1}) to the larger Δp which must be positive ($+1.37 \pm 0.04$ mm s^{-1}) and site 1 ($2\varepsilon \sim +0.27$ mm s^{-1}) to the smaller Δp which must be negative (-1.08 ± 0.04 mm s^{-1}). In agreement with electronic structure calculations, the quadrupole interactions at the Sn inequivalent crystallographic sites are deduced to be of opposite sign and, consistently, sites 1 and 2 correspond to Sn1 and Sn2 nuclei, respectively. We note that the hyperfine field B_{hf} on the Sn1 nuclei is significantly larger than that experienced by the Sn2 nuclei.

TABLE V. ^{119}Sn hyperfine interaction parameters of Mn_3Sn_2 for $T<T_t$ with fixed φ values ($\varphi=90°$ and $\varphi=0°$ for site 1 and 2, respectively, see text). The $1'$ and $2'$ sites correspond to Sn nuclei with hyperfine fields still along the b axis ($\theta=90°$ and $\varphi=0°$ for site $1'$; $\theta=90°$ and $\varphi=90°$ for site $2'$). P is the relative area of the corresponding subspectrum.

T (K)	Site	P ±0.03	Γ (mm s^{-1}) ±0.06	IS (mm s^{-1}) ±0.08	Δ (mm s^{-1}) ±0.08	B_{hf} (kG) ±3	η ±0.1	θ (deg) ±5
190	1	0.41	1.14	1.92	−0.95	173	0.3	56
	2	0.37	1.14	2.02	1.25	149	0.6	59
	$1'$	0.11	1.14	1.92	−0.95	167	0.3	90
	$2'$	0.12	1.14	2.02	1.25	136	0.6	90
180	1	0.40	1.16	1.93	−1.03	178	0.3	56
	2	0.46	1.16	2.02	1.17	156	0.6	59
	$1'$	0.07	1.16	1.93	−1.03	171	0.3	90
	$2'$	0.05	1.16	2.02	1.17	141	0.6	90
160	1	0.51	1.17	1.92	−1.02	187	0.3	57
	2	0.49	1.17	2.01	1.18	164	0.7	61
140	1	0.51	1.18	1.91	−1.02	194	0.3	57
	2	0.49	1.18	2.01	1.17	170	0.8	63
120	1	0.51	1.16	1.91	−1.09	201	0.2	59
	2	0.49	1.16	2.03	1.19	176	0.7	61
100	1	0.51	1.17	1.92	−1.02	208	0.3	58
	2	0.49	1.17	2.02	1.17	182	0.8	61
50	1	0.50	1.14	1.99	−1.09	217	0.3	59
	2	0.50	1.14	2.09	1.17	189	0.7	61
5	1	0.50	1.19	2.00	−1.09	219	0.2	59
	2	0.50	1.19	2.09	1.18	192	0.7	61

Results of our second set of fits at temperatures above T_t are gathered in Table IV. They were carried out beyond the first-order approximation using the fixed θ and φ values given above. They yield $\Delta\sim-1.0$ mm s^{-1} and $\eta\sim0.4$ for Sn1, while $\Delta\sim+1.2$ mm s^{-1} and $\eta\sim0.8$ for Sn2. For temperatures below T_t, the hyperfine fields are along the c axis. Hence, $\varphi=90°$ and 0° for, respectively, Sn1 and Sn2 while the θ values depend on the exact orientation of the principal Z axes within the ac plane. Results of our fittings below 200 K, which were carried out fixing the φ angles to 90° and 0° while the θ values were let free to vary, are given in Table V. For both sites, they show that, as expected, Δ and η have not significantly changed compared to their values above T_t and yield θ angles close to 60°. Since the hyperfine fields are directed along the c axis, these θ values are fully consistent with the computed α_1 and α_2 angles giving the orientation of two of the EFG principal axes relative to the crystal axes [Fig. 8(b)].

We noticed that the fittings of the spectra at 190 and 180 K are improved if we consider that a small fraction of the Sn nuclei have still their hyperfine field directed along the b axis. Four subspectra were then used: two for the Sn nuclei with B_{hf} still along the b axis (site $1'$ and $2'$) and two for the nuclei with B_{hf} along the c axis (site 1 and 2). We found that ~25% and ~10% of the Sn nuclei have still their hyperfine field directed along the b axis at 190 and 180 K, respectively. This is interpreted as being due to a certain spread in the reorientation temperature of the hyperfine field (i.e., of the Mn moments) which rotates abruptly from the b axis to the c axis upon cooling. This spread in the reorientation temperature might be caused by local compositional and/or microstructural variations. The dependence of the B_{hf} values on their orientation is a direct manifestation of the anisotropic contributions.

IV. DISCUSSION AND CONCLUSION

Refinements of our powder neutron-diffraction data have allowed determining the magnetic structure of Mn_3Sn_2 in the three temperature domains. To summarize:

(i) The spins of both the Mn 8d and Mn 4c are ferromagnetically aligned along the b axis between T_{C1} and T_{C2}.

(ii) Between T_{C2} and T_t, the Mn 8d spins adopt a canted ferromagnetic structure, due to a ferromagnetic component along the b axis and an antiferromagnetic one along the a axis, while the Mn 4c moments are still ferromagnetically aligned along the b axis.

(iii) Below T_t, the ferromagnetic components of both Mn 4c and Mn 8d lie along the c axis while the antiferromagnetic component of Mn 8d remains along the a axis.

These magnetic arrangements are confirmed by the ^{119}Sn Mössbauer analysis. In addition, the Mössbauer spectra re-

corded near T_t suggest that the spin reorientation toward the c axis takes place abruptly but with a certain spread in the reorientation temperature of the individual spins.

The qualitative analysis of the in-field neutron data (Fig. 7) has led to the conclusion that the canted ferromagnetic arrangement of the Mn 8d magnetic moment is not significantly altered by applied magnetic field as large as 1.5 T. For this applied magnetic field value, the magnetization of Mn_3Sn_2 is almost saturated, close to its value under 5 T (see Fig. 2 of Ref. 1). This indicates that, even in large magnetic fields, the canting angle is almost unchanged. The preservation of the canted structure in large fields is verified through the close proximity between the magnetization deduced from zero-field neutron refinements and the macroscopic magnetization measured in a 3 T magnetic field shown in the inset of Fig. 6 (the latter data were taken from Ref. 1). The magnetization increase and the MCE peak previously observed at T_{C2} (Refs. 1 and 2) are therefore solely due to the zero-field ferromagnetic components (i.e., they are not linked to a field-induced closing of the canting angle) and obviously cannot be accounted for by the appearance of the antiferromagnetic component on Mn 8d. Figure 6 shows that the appearance of the antiferromagnetic component (A_x mode) of the Mn 8d magnetic moment at T_{C2} is accompanied by a slight but perceptible increase in its ferromagnetic component, while there is no anomaly in the temperature dependence of the still larger Mn 4c magnetic moment. We further note that Mn 4c and Mn 8d have identical magnetic configurations above T_{C2} (F_y and F_{By} modes) but not below (F_y and $F_{By}A_{Bx}$ modes, respectively). Taken together, these remarks lead to the conclusion that the ferromagneticlike transitions at T_{C1} and T_{C2} are due to the two Mn sites ordering separately. At T_{C1}, the Mn 4c site orders in a collinear ferromagnetic arrangement (F_y) which polarizes the Mn 8d atoms due to intersite coupling. The Mn 8d sublattice orders cooperatively at T_{C2} in a canted ferromagnetic structure ($A_{Bx}F_{By}$) belonging to the same irreducible representation than the F_y mode of Mn 4c. Hence, the transition at T_{C2} is a disorder-order transformation. This explains the second-order features of this transition previously observed by macroscopic measurements: lack of thermal and field hysteresis in the magnetization,[1] shape and field dependences of both the magnetic entropy change[1] and specific heat[2] peaks. The separate magnetic ordering of transition metal atoms in intermetallics, an uncommon event, has been reported for instance in monoclinic FeGe.[31]

Upon further cooling below T_t, the ferromagnetic components of Mn 4c and Mn 8d reorient toward the c axis. This transition was previously ascribed to a weak supplementary antiferromagnetic interaction.[1] However, our neutron refinements do not evidence the appearance of a supplementary antiferromagnetic component nor the reduction of the ferromagnetic ones (Fig. 6). We are then led to conclude that the transition at T_t just involves a spin reorientation and does not alter the microscopic magnetization. Interestingly, the A_{Bx} and F_{Bz} modes of Mn 8d are found to belong to different irreducible representations (i.e., magnetic space groups). This is often an indication that high-order terms, beyond the usual Heisenberg bilinear exchange coupling, must be unusually large and have to be included in the spin Hamiltonian.[15,16,32,33] These high-order non-Heisenberg terms could be biquadratic or multispin exchange mechanisms.[34,35] An alternative explanation could come from a lowering of symmetry. The two involved magnetic space groups $Pn'ma'$ and $Pn'm'a$ have the intersection $P2_1'/n'11$ (the global magnetic symmetry). In the monoclinic $P2_1/n11$ space group (notice the nonconventional setting), the 8d position of $Pnma$ splits into two sites both in the 4e general position. The 4c position of $Pnma$ also transforms to 4e position. In $P2_1/n11$ there are four irreducible representations associated with $\mathbf{k}=(0\ 0\ 0)$,[36] the relevant one admits the A_x, F_y, and F_z modes for the 4e position (using the numbering given in Table II). Thus, in the monoclinic $P2_1/n11$ space group the observed A_x and F_z modes are found to belong to the same irreducible representation. This suggests that Mn_3Sn_2 might undergo a very weak (undetected) monoclinic distortion below T_t. Finally, Izyumov and co-workers[37,38] identified another possible mechanism for observing combined irreducible representations (the exchange multiplets), but it needs weak anisotropic interactions. Further works are required to understand the origin of the behavior of Mn_3Sn_2 below T_t.

The spin reorientation at T_t allows observing that the transferred hyperfine fields at Sn nuclei are partially anisotropic. An estimate of the magnitude of the anisotropic contributions can be obtained as follows. Assuming an axially symmetric hyperfine coupling tensor, the hyperfine field collinear to the magnetization can be written to first order by

$$B_{hf} = B_{iso} + B_{aniso}\left(\frac{3\cos^2\theta - 1}{2}\right), \tag{3}$$

where B_{iso} and B_{aniso} are, respectively, the isotropic and anisotropic parts of the total hyperfine field B_{hf}.[23] We further assume that B_{hf} is negative (i.e., opposite to the Mn moment direction) as in $RMn_6Sn_{6-x}X_x$.[21,22,25] From the 190 K data (Table V), we found

$$B_{iso} \sim -173 \text{ kG and } B_{aniso} \sim -13 \text{ kG for Sn1},$$

$$B_{iso} \sim -152 \text{ kG and } B_{aniso} \sim -33 \text{ kG for Sn2}.$$

In both cases, the isotropic and anisotropic contributions have the same sign in Mn_3Sn_2, as also observed in $RMn_6Sn_{6-x}X_x$.[22] The ratio of anisotropic to isotropic fields is calculated to be ~7.5% and ~21.7% for Sn1 and Sn2, respectively. These ratios point to a less spherical 5p spin density on the Sn2 atoms since these anisotropic fields are expected to be mainly from dipolar origin. Anisotropic fields of comparable relative amount have been reported in $RMn_6Sn_{6-x}X_x$.[22] The EFG experienced by the Sn1 and Sn2 nuclei are of opposite sign. The higher value of the quadrupolar interaction at the Sn2 nuclei indicates that the 5p charge density is less spherical on the Sn2 atoms.[25] These differences in the anisotropy of the charge and spin densities as well as in the magnitude of B_{hf} are manifestations of the dissimilarity in the way the two Sn sites are coordinated by Mn 4c atoms, since their trigonal Mn 8d prismatic environments are very resembling [see Fig. 8(a) and Sec. III B].

To conclude, we have determined the magnetic structure of the magnetocaloric Mn_3Sn_2 compound and have identified the origin of the three magnetic transitions previously observed from macroscopic measurements. The magnetic behavior of Mn_3Sn_2 is somewhat unusual: the two nonequivalent Mn sites order separately and the m_x and m_z components of the Mn 8*d* moment are found to belong to different irreducible representations below T_t, suggesting that high-order terms beyond the bilinear spin-spin interactions determine the magnetic ground state or that a very small (undetected) lowering of symmetry takes place below T_t. We expect that the atypical magnetic behavior of Mn_3Sn_2 will motivate further theoretical and experimental investigations. Noncollinear band structure calculations are in progress.

ACKNOWLEDGMENTS

We are indebted to the Institut Laue Langevin (Grenoble, France) for the provision of research facility. We thank our local contact (O. Isnard) for his help during the recording of the neutron data. We acknowledge D. Malterre (IJL, Nancy, France) for enlightening discussions on group theory. We are grateful to one of the referees for pointing out the possible lowering to monoclinic symmetry below T_t.

*Corresponding author; thomas.mazet@lcsm.uhp.nancy.fr

[1] T. Mazet, H. Ihou-Mouko, and B. Malaman, Appl. Phys. Lett. **89**, 022503 (2006).
[2] Q. Recour, T. Mazet, and B. Malaman, J. Appl. Phys. **105**, 033905 (2009).
[3] K. A. Gschneidner, Jr., V. K. Pecharsky, and A. O. Tsokol, Rep. Prog. Phys. **68**, 1479 (2005).
[4] E. Brück, J. Phys. D: Appl. Phys. **38**, R381 (2005).
[5] K. A. Gschneidner, Jr. and V. K. Pecharsky, Int. J. Refrig. **31**, 945 (2008).
[6] R. Zeng, L. Lu, W. X. Li, J. H. Kim, D. Q. Shi, H. K. Liu, S. X. Dou, J. L. Wang, S. J. Campbell, Z. Wang, Y. Li, M. Y. Zhu, and C. Q. Feng, J. Appl. Phys. **105**, 07A935 (2009).
[7] Phase Equilibria, in *Crystallographic and Thermodynamic Data of Binary Alloys*, Landolt-Börnstein, New series, Group IV Vol. 5H, edited by B. Predel (Springer-Verlag, Berlin, 1997).
[8] M. Stange, H. Fjellvåg, S. Furuseth, and B. C. Hauback, J. Alloys Compd. **259**, 140 (1997).
[9] M. Elding-Pontén, L. Stenberg, A. K. Larsson, S. Lidin, and K. Ståhl, J. Solid State Chem. **129**, 231 (1997).
[10] C. G. Shull, W. A. Strauser, and E. O. Wollan, Phys. Rev. **83**, 333 (1951).
[11] L. M. Corliss and J. M. Hastings, J. Appl. Phys. **34**, 1192 (1963).
[12] J. Rodriguez-Carvajal, Physica B **192**, 55 (1993).
[13] L. B. McCusker, R. B. Von Dreele, D. E. Cox, D. Loüer, and P. Scardi, J. Appl. Crystallogr. **32**, 36 (1999).
[14] G. Le Caër (private communication).
[15] E. F. Bertaut, Acta Crystallogr., Sect. A: Found. Crystallogr. **24**, 217 (1968).
[16] E. F. Bertaut, in *Magnetism*, edited by H. Suhl and G. Rado (Academic Press, New York, 1963), Vol. III, p. 186.
[17] P. Schobinger-Papamantellos, J. Phys. Chem. Solids **39**, 197 (1978).
[18] T. Ericsson and R. Wäppling, J. Phys. Colloq. **37**, C6-719 (1976).
[19] C. Hohenemser, Phys. Rev. **139**, A185 (1965).
[20] G. Le Caër, B. Malaman, G. Venturini, and I. B. Kim, Phys. Rev. B **26**, 5085 (1982).
[21] T. Mazet, J. Tobola, G. Venturini, and B. Malaman, Phys. Rev. B **65**, 104406 (2002).
[22] L. K. Perry, D. H. Ryan, and G. Venturini, Phys. Rev. B **75**, 144417 (2007).
[23] S. K. Kulshreshtha and P. Raj, J. Phys. F: Met. Phys. **12**, 377 (1982).
[24] P. Blaha, K. Schwarz, and P. Herzig, Phys. Rev. Lett. **54**, 1192 (1985).
[25] T. Mazet, H. Ihou-Mouko, J. F. Marêché, and B. Malaman, Eur. Phys. J. B **51**, 173 (2006).
[26] D. Torumba, V. Vanhoof, M. Rots, and S. Cottenier, Phys. Rev. B **74**, 014409 (2006).
[27] P. Blaha, K. Schwarz, G. Madsen, D. Kvasnicka, and J. Luitz, *Wien2k: An Augmented Plane Wave + Local Orbitals Program for Calculating Crystal Properties*, edited by Karlheinz Schwarz (Technische Universität, Wien, Austria, 1999).
[28] A preliminary account of the electronic structure of Mn_3Sn_2 based on collinear computations has been given in a conference talk: J. Tobola, T. Mazet, Q. Recour, and B. Malaman, Euromat Congress (unpublished). A detailed electronic structure study including noncollinear calculations will be published elsewhere.
[29] H. Haas, M. Menningen, H. Andreasen, S. Damgaard, H. Grann, F. T. Pedersen, J. W. Petersen, and G. Weyer, Hyperfine Interact. **15**, 215 (1983).
[30] G. Le Caër, J. M. Dubois, L. Häggström, and T. Ericsson, Nucl. Instrum. Methods **157**, 127 (1978).
[31] D. Fruchart, B. Malaman, G. Le Caër, and B. Roques, Phys. Status Solidi A **78**, 555 (1983).
[32] M. Reehuis, C. Ulrich, P. Pattison, B. Ouladdiaf, M. C. Rheinstädter, M. Ohl, L. P. Regnault, M. Miyasaka, Y. Tokura, and B. Keimer, Phys. Rev. B **73**, 094440 (2006).
[33] M. Reehuis, C. Ulrich, P. Pattison, M. Miyasaka, Y. Tokura, and B. Keimer, Eur. Phys. J. B **64**, 27 (2008).
[34] C. Herring, in *Magnetism*, edited by H. Suhl and G. Rado (Academic Press, New York, 1966), Vol. IIB, p. 1.
[35] E. L. Nagaev, Sov. Phys. Usp. **25**, 31 (1982).
[36] G. Rousse, J. Rodriguez-Carvajal, C. Wurm, and C. Masquelier, Chem. Mater. **13**, 4527 (2001).
[37] Yu. A. Izyumov and V. E. Naish, J. Magn. Magn. Mater. **12**, 239 (1979).
[38] Yu. A. Izyumov, V. E. Naish, and S. B. Petrov, J. Magn. Magn. Mater. **13**, 275 (1979).